JOURNAL OF AIRCRAFT
Vol. 36, No. 3, May–June 1999

Unsteady Aerodynamic Characteristics of Airfoil with Moving Spoilers

C. Xu* and W. W. H. Yeung†
Nanyang Technological University, Singapore 639798, Republic of Singapore

A discrete vortex model is developed for simulating unsteady separated flow around an airfoil with a conventional or base-vented spoiler when the spoiler is deployed at a finite speed. The airfoil and spoiler are discretized by linear segments. A linear distribution of vortices and a constant source are used to represent each segment, forming the basis of the present method. Discrete vortices are shed from each separation point. A new sharp-edge condition is formulated such that the location and strength of the nascent vortex near a separation point are determined by means of the continuity equation and the momentum principle. A method to model the moving surface is also presented. The no-slip condition and a diffusion scheme were incorporated into the numerical simulation for simulating the flow around the base-vented spoiler. The computed results are compared with those of other methods and with experimental results for the conventional spoiler. The computation of a base-vented spoiler shows that base venting can reduce the adverse effect when the spoiler undergoes rapid deployment. The comparison indicates that the present method provides reasonable results.

Nomenclature

A_{pq}, A'_{pq}	= influence coefficients
a_k	= coefficients for series
B_{pq}, B'_{pq}	= influence coefficients
C_L	= lift coefficient
C_{La}	= adverse lift coefficient
C_p	= pressure coefficient
C_{pq}, C'_{pq}	= influence coefficients
c	= chord of the airfoil
D	= domain
D_{pq}	= influence coefficient
l	= length of element
m	= number of shed vortices
N	= number of nodal points
$\boldsymbol{n}$	= normal unit vector
n_t	= number of terms in series
p	= pressure
Q	= total velocity
Re	= Reynolds number
r	= radius
r_0	= radius of vortex blob
s	= control surface
T	= nondimensional time
T_a	= time reach onset of lift
T_b	= time to reach maximum lift
t	= time
U_∞, V_∞	= freestream velocity
x, y	= global coordinates
Z	= length of nascent vortex sheet
z	= distance between two vortices
α	= airfoil incidence
β	= half-angle of trailing edge
Γ	= circulation of vortex
γ	= strength of vortex
Δ	= difference
δ	= spoiler deployment angle
ε	= error of calculation
η, ξ	= local coordinates
λ	= complex term
ν	= kinematic viscosity
ρ	= density of fluid
σ	= source strength
Φ	= velocity potential
φ	= vortex shedding angle
ψ	= stream function
ω	= vorticity or angular speed

Subscripts

f	= airfoil
i, j, p, q	= running indices
$N, N-1$	= upper surface elements at trailing edge
s	= shed vortex
tip	= tip of the sharp edge
w	= wake
0	= nascent vortex or initial time
1, 2	= lower surface elements at trailing edge
∞	= freestream

Received May 1, 1998; revision received Jan. 4, 1999; accepted for publication Jan. 5, 1999.

*Ph.D. Candidate, School of Mechanical and Production Engineering; currently on sabbatical at Mechanical Engineering Department, University of Wisconsin, Milwaukee, WI 53211.

†Senior Lecturer, School of Mechanical and Production Engineering.

I. Introduction

IN the development of new aircraft, much attention is given to the time-dependent aerodynamic characteristics of the control surfaces. Time-dependent separated flows with moving boundaries, such as the flow around an airfoil with a moving spoiler, are generally difficult to compute by using the Navier–Stokes equations.[1] To obtain engineering solutions for these types of flow problems, simpler mathematical models are often used. The panel method is one of the most economical models for separated flow calculation. In this study, the panel method has been extended to solve the moving spoiler problem.

Recently, Tou and Hancock[2] used the panel method to model the unsteady flow around an airfoil with a stationary spoiler. However, their method was found to be unsuitable for the flow around a moving spoiler, as concluded in the study. Computed results of the lift variation with time are highly irregular when the deployment angle of the spoiler is small, mainly because the method cannot satisfactorily deal with reattached flow behind the spoiler. Bearman et al.[3] used conformal mapping to study the stationary and moving conventional spoiler problems. However, the conformal mapping method is difficult to extend to three-dimensional flow simulation. Developing a panel method to simulate the unsteady flow around an airfoil with a conventional spoiler is still a challenge to aerodynamicists. The objective of the present investigation is to develop

numerical methods to study the unsteady flow around an airfoil with a conventional or base-vented spoiler.

Models combining the panel method and the discrete vortex method are developed for unsteady separated incompressible flow around an airfoil with a conventional spoiler. Special features in the two present models include the introduction of a nascent vortex sheet at each sharp edge for vortex shedding, splitting of the vortices when the distance between two neighboring vortices is greater than five times the distance between the trailing edge and its nascent vortex, and the introduction of the vortex-blob concept to include the transient and viscous effects. The shed vortices form the wake behind the spoiler and airfoil trailing edge are convected downstream. This method tracks the trajectory of each vortex as a function of time since its creation in the flowfield. The calculated results show that when the spoiler is extended, qualitative trends of the lift C_L are similar to the results of experimental measurements.[4,5] The influence of the spoiler deployment rates on the transient lift has also been investigated, and the flowfield behind the spoiler was obtained.

The adverse lift effect may be significant even in the case of a moderate rate of spoiler rotation. It can be as large as 50% of the net change in lift.[5] This effect may influence the aircraft behavior during landing. A method is proposed to reduce this initial increase in lift by creating another starting vortex whose sense of rotation is opposite to that created by the conventional spoiler. This can be achieved by simply introducing a gap between the spoiler and the airfoil such that a counter-rotating vortex pair is shed from the upper and the lower tips of the spoiler. The initial increase in lift on the airfoil will diminish because of the reduction in net circulation of the vortex pair. Although some experimental investigation associated with the unsteady flow around a base-vented spoiler has been conducted, as reported by Yeung et al.,[6] the computational aspect of this kind of flow is limited in the literature.

The flow around an airfoil with a base-vented spoiler is more complicated than flow past a conventional spoiler because the flow that separates from the lower tip of the spoiler may be strongly influenced by the boundary-layer separation on the airfoil upstream of the spoiler. The construction of the present numerical model takes this aspect of flow into consideration. The no-slip vortex scheme was developed to solve the flow around an airfoil with a base-vented spoiler when a spoiler is opened at a finite speed. The computed flow patterns with different time steps were obtained, and the computed results are compared with experimental results and flow visualizations.[7]

II. Mathematical Model

A. Method of Solution

The computational method presented here involves four stages. The first stage is the potential flow calculation, in which the surfaces of the airfoil and spoiler are discretized into panels. Each panel is represented by a linear piecewise vortex and a constant source, with their strengths determined by satisfying the normal flow condition at the control point. Then, the unsteady separated flow associated with an airfoil and a rapidly extended spoiler is calculated by using the discrete vortex method involving the other three stages, namely, vortex shedding, convection, and diffusion. To establish the condition of normal velocity at each point, the velocity potential and velocities influenced by singularities need to be constructed.

The influence at point $P(\xi_p, \eta_p)$ from a vortex distribution of strength γ located between ξ_q and ξ_{q+1} is an integral of the influence from this element q. Therefore,

$$\Phi_p = \frac{1}{2\pi}\int_{\xi_q}^{\xi_{q+1}} \gamma \tan^{-1}\frac{\eta_p}{\xi_p - \xi}\,\mathrm{d}\xi \tag{1}$$

$$u_p = \frac{1}{2\pi}\int_{\xi_q}^{\xi_{q+1}} \gamma \frac{\eta_p}{(\xi_p - \xi)^2 + \eta_p^2}\,\mathrm{d}\xi \tag{2}$$

$$v_p = \frac{1}{2\pi}\int_{\xi_q}^{\xi_{q+1}} \gamma \frac{\xi_p - \xi}{(\xi_p - \xi)^2 + \eta_p^2}\,\mathrm{d}\xi \tag{3}$$

Consider a linear vortex distribution along the ξ axis. If its strength varies from γ_q at ξ_q to γ_{q+1} at ξ_{q+1}, its influence at point P is obtained by integrating Eqs. (1–3). As a result

$$\Phi_p = -\frac{\gamma_q}{2\pi}\left[(\xi_p - \xi_q)\theta_q - (\xi_p - \xi_{q+1})\theta_{q+1} + \eta_p \ln\frac{r_q}{r_{q+1}}\right] - \frac{\gamma_{q+1} - \gamma_q}{4\pi(\xi_{q+1} - \xi_q)}\left[\left(\xi_p^2 - \eta_p^2 - \xi_q^2\right)\theta_q - \left(\xi_p^2 - \eta_p^2 - \xi_{q+1}^2\right)\theta_{q+1} + 2\xi_p\eta_p \ln\frac{r_q}{r_{q+1}} + \eta_p(\xi_q - \xi_{q+1})\right] \tag{4}$$

$$u_p = \frac{\eta_p}{2\pi}\left(\frac{\gamma_{q+1} - \gamma_q}{\xi_{q+1} - \xi_q}\right)\ln\frac{r_{q+1}}{r_q} + \frac{\gamma_q(\xi_{q+1} - \xi_q) + (\gamma_{q+1} - \gamma_q)\xi_p}{2\pi(\xi_{q+1} - \xi_p)}(\theta_{q+1} - \theta_q) \tag{5}$$

$$v_p = \frac{\eta_p}{2\pi}\left(\frac{\gamma_{q+1} - \gamma_q}{\xi_{q+1} - \xi_q}\right)\left[(\theta_{q+1} - \theta_q) + \frac{(\xi_{q+1} - \xi_q)}{\eta_p}\right] + \frac{\gamma_q(\xi_{q+1} - \xi_q) + (\gamma_{q+1} - \gamma_q)(\xi_p - \xi_q)}{2\pi(\xi_{q+1} - \xi_q)}\ln\frac{r_{q+1}}{r_q} \tag{6}$$

where

$$\theta_k = \tan^{-1}[\eta_p/(\xi_p - \xi_k)], \qquad k = q, q+1$$

$$r_k^2 = (\xi_p - \xi_k)^2 + \eta_p^2, \qquad k = q, q+1$$

These equations were used in the present numerical analysis in representing the airfoil surface. Similarly, the velocity components and velocity potential at point P for a source of strength σ located at $(\xi, 0)$ in Cartesian coordinates are

$$\Phi_p = (1/2\pi)\sigma \ln\sqrt{(\xi_p - \xi)^2 + \eta_p^2} \tag{7}$$

$$u_p = \frac{1}{2\pi}\sigma\frac{\xi_p - \xi}{(\xi_p - \xi)^2 + \eta_p^2} \tag{8}$$

$$v_p = \frac{1}{2\pi}\sigma\frac{\eta_p}{(\xi_p - \xi)^2 + \eta_p^2} \tag{9}$$

Consider the source distribution along the ξ axis in a local coordinate system (ξ, η). The influence of this distribution at point P is an integral of the influence of the continuous source from Eqs. (7–9):

$$\Phi_p = \frac{1}{2\pi}\int_{\xi_p}^{\xi_{q+1}} \sigma \ln\sqrt{(\xi_p - \xi)^2 + \eta_p^2}\,\mathrm{d}\xi \tag{10}$$

$$u_p = \frac{1}{2\pi}\int_{\xi_p}^{\xi_{q+1}} \sigma\frac{\xi_p - \xi}{(\xi_p - \xi)^2 + \eta_p^2}\,\mathrm{d}\xi \tag{11}$$

$$v_p = \frac{1}{2\pi}\int_{\xi_p}^{\xi_{q+1}} \sigma\frac{\eta_p}{(\xi_p - \xi)^2 + \eta_p^2}\,\mathrm{d}\xi \tag{12}$$

The boundary condition of zero normal velocity is imposed at the control point of each panel. The velocity formulas in Eqs. (8), (9), (11), and (12) are used to calculate the induced velocity. A system of linear equations results:

$$\sum_{q=1}^{N+N_w} A_{pq}\gamma_q + \sigma\sum_{q=1}^{N} B_{pq} = -(U_\infty + u_w, V_\infty + v_w)\cdot\boldsymbol{n}_p \tag{13}$$

The velocity components induced by the wake vortices u_w and v_w, can be calculated by

$$u_w = \sum u_{pm}, \qquad v_w = \sum v_{pm} \qquad (m = 1, \ldots, N_s) \tag{14}$$

where

$$u_{pm} = \Gamma_m \frac{1}{2\pi}\left[\frac{y_p - y_m}{(x_p - x_m)^2 + (y_p - y_m)^2}\right]$$

$$v_{pm} = -\Gamma_m \frac{1}{2\pi}\left[\frac{x_p - x_m}{(x_p - x_m)^2 + (y_p - y_m)^2}\right]$$

In addition, Kelvin's theorem has been used for keeping the sum of the circulation around the body and wake constant. That is

$$\frac{\mathrm{d}\Gamma}{\mathrm{d}t} = \frac{\Delta(\Gamma_{\text{airfoil-spoiler}} + \Gamma_{\text{wake}})}{\Delta t} = 0 \tag{15}$$

The advance of each free vortex in location is calculated from the following finite difference equations, as suggested by Clements and Maull[8]:

$$x(t + \Delta t) = x(t) + 1.5\Delta t u(t) - 0.5\Delta t u(t - \Delta t) \tag{16}$$

$$y(t + \Delta t) = y(t) + 1.5\Delta t v(t) - 0.5\Delta t v(t - \Delta t) \tag{17}$$

B. Sharp-Edge Conditions

The usual assumption in inviscid analysis to deal with sharp edges is that the net force cannot be sustained across the fluid element joining the sharp edge and its concentrated vortex, as employed by Edwards and Cheng.[9] This enables the determination of the position and strength of the concentrated vortex. Hsu and Wu[10] introduced a scheme for shed vortex interaction based on the momentum principle in the study of the blade–vortex. The present study employs the assumption in Ref. 9 and extends the model in Ref. 10 to separated flow.

Consider the case of the conventional spoiler in Fig. 1. To determine the position of the nascent vortex sheet near the sharp edge, the flow direction and velocity along the vortex sheet downstream of the sharp edge should be determined. Suppose that the flow separates at the sharp edge and the boundary layers of finite thickness are represented by a vortex sheet of zero thickness. The flow approaching the trailing edge on both surfaces of the sharp edge will tend to zero in the direction normal to the sheet. In the unsteady separated flow, the wake vortex sheet is, in general, not parallel to either the upper or lower surface of the sharp edge. Applying the momentum theorem to an infinitesimal control volume in Fig. 2 gives

$$\int_s \rho Q(Q \cdot \mathrm{d}s) = 0 \tag{18}$$

Equation (18) can be written as two scalar equations in the ξ and η directions.

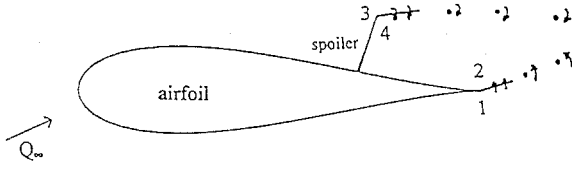

Fig. 1 Separated flow model for airfoil/spoiler.

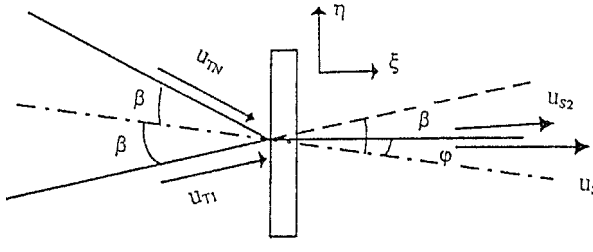

Fig. 2 Control volume near the trailing edge.

If the net force across the sheet is zero, the momentum equation on an infinitesimal control volume in the η direction is

$$u_{T1}^2 \sin^2(\beta - \varphi) - u_{TN}^2 \sin^2(\beta + \varphi) = 0 \tag{19}$$

where u_{T1} and u_{TN} are the tangential velocities of the flow at control points 1 and N, as indicated in Fig. 2. The quantities 2β and φ are, respectively, the sharp-edge angle and inclination of the nascent-vortex sheet with respect to the angle bisector of the sharp edge.

If $u_{T1}\sin(\beta - \varphi) - u_{TN}\sin(\beta + \varphi) = 0$, then

$$\tan\varphi = [(u_{T1} - u_{TN})/(u_{T1} + u_{TN})]\tan\beta \tag{20}$$

But, if $u_{T1}\sin(\beta - \varphi) + u_{TN}\sin(\beta + \varphi) = 0$, then

$$\tan\varphi = [(u_{T1} + u_{TN})/(u_{T1} - u_{TN})]\tan\beta \tag{21}$$

Equation (20) (for $\varphi < \beta$) is reduced to Eq. (21) (for $\varphi < \beta$) if u_{TN} is negative. Therefore, either Eq. (20) or (21) can be used.

For a sufficiently small control volume, the continuity equation can be written as

$$\int_s \rho Q \cdot \mathrm{d}s = 0 \tag{22}$$

Applying the continuity equation to a sharp edge yields

$$u_{S1} + u_{S2} = u_{TN}\cos(\beta + \varphi) + u_{T1}\cos(\beta - \varphi) \tag{23}$$

Using the fact that the nascent vortex sheet moves with the local velocity of the shear layer, the length of the sheet is given by

$$l = (u_{S1} + u_{S2})\Delta t/2 \tag{24}$$

The strength can be expressed as a function of the tangential velocities across the sheet, and is equal to

$$u_{TN} = (\gamma_{N-1} + \gamma_N)/2 \tag{25}$$

$$u_{T1} = (\gamma_1 + \gamma_2)/2 \tag{26}$$

Equations (20) and (24) permit the inclination and length of the nascent vortex sheet to be determined. It is important to point out that the present sharp-edge flow model is established based on a viscous flow analysis. It cannot be obtained on the basis of potential flow analysis.

C. Unsteady Kutta Pressure Condition

After determining the inclination and length of a nascent vortex sheet, the unsteady Kutta pressure condition is used to determine its strength. In the present analysis, the sheet having a circulation Γ_{m0} is allowed to change with time. This requires the feeding of vorticity, and results in a nonvanishing pressure across the sheet. If the length of the nascent vortex sheet is $2Z$, the force on the sheet according to Ref. 9 is given by

$$F = -\rho\frac{\mathrm{d}\Gamma_{m0}}{\mathrm{d}t}Z = \rho V^*\Gamma_{m0} = 0 \tag{27}$$

where V^* is the velocity of the local flow at the midpoint of nascent vortex sheet. Therefore,

$$\left[\frac{\mathrm{d}(\gamma_{\text{tip}} + \gamma_{w0})}{\mathrm{d}t}Z + (\gamma_{\text{tip}} + \gamma_{w0})\frac{\mathrm{d}Z}{\mathrm{d}t}\right] = (\gamma_{\text{tip}} + \gamma_{w0})V^* \tag{28}$$

where $\Gamma_{m0} = 2Z(\gamma_{\text{tip}} + \gamma_{w0})$.

At each time step, it is necessary to invoke a Kutta pressure condition linking the pressures at the spoiler tip and trailing edge. The outside and inside of the wake element at the airfoil trailing edge are numbered 1 and 2, respectively, whereas 3 and 4 are for those at the spoiler tip (Fig. 1). From the unsteady Bernoulli's equation between 1 and 3:

$$p_1 + \frac{1}{2}\rho Q_1^2 + \rho\frac{\partial\Phi_1}{\partial t} = p_3 + \frac{1}{2}\rho Q_3^2 + \rho\frac{\partial\Phi_3}{\partial t} \tag{29}$$

Hence,

$$p_3 - p_1 = -\rho\left[\frac{(Q_3 + Q_1)}{2}(Q_3 - Q_1) + \frac{\partial(\Phi_3 - \Phi_1)}{\partial t}\right] \quad (30)$$

Applying Bernoulli's equation from side 4 to side 2,

$$p_4 - p_2 = -\rho\left[\frac{(Q_4 + Q_2)(Q_4 - Q_2)}{2} + \frac{\partial(\Phi_4 - \Phi_1)}{\partial t}\right] \quad (31)$$

The Kutta pressure difference condition can be written as

$$p_3 - p_1 = p_4 - p_2 \quad (32)$$

Equation (32) is a nonlinear equation involving γ and σ, and can be solved by using the Newton–Raphson scheme.[11] Equations (28) and (32) permit the strength of a nascent vortex sheet to be determined.

In the calculation by Kim and Mook,[12] the condition of vortex strength at the sharp-edge point is equal to zero and a wake vortex of unknown strength is placed there. This implies that their algebraic equations require an optimization technique to produce a deterministic system. Here, this condition is replaced by a new condition that the velocity gradients along the upper and lower surfaces are the same, i.e.,

$$\left(\frac{\partial \gamma}{\partial l}\right)_u = \left(\frac{\partial \gamma}{\partial l}\right)_l \quad (33)$$

The second-order backward-differencing scheme is used to solve Eq. (33).

D. Moving Surface

The following describes the mathematical formulation of a body with a moving surface. The continuity equation in terms of the velocity potential Φ is

$$\nabla^2 \Phi = 0 \quad (34)$$

Note that Eq. (34) does not include the time derivative, but is introduced through the boundary condition. Let the coordinate system (X, Y) be fixed to the airfoil, and the spoiler rotation rate in the airfoil frame be ω. The position vector from the spoiler hinge point to any other point on the spoiler is r. The normal boundary condition, which requires zero normal velocity at each point P on the body, is satisfied by the following equation:

$$(\nabla \Phi - \omega \times r)_p \cdot \boldsymbol{n}_p = 0 \quad (35)$$

The incompressible continuity equation in the integral form states that the change in mass within a closed boundary is zero:

$$\int_{s_b} \rho \nabla \Phi \cdot \boldsymbol{n}\, \mathrm{d}s = 0 \quad (36)$$

If the surface S_b represents a solid surface, then the internal mass is unchanged, i.e.,

$$\Phi_{\text{in}} = 0 \quad (37)$$

A discontinuity in the velocity field may be represented by a source distribution. In this way, the moving surface can be seen as a distribution of sources in which the velocity component normal to the surface is determined by the strength of the source at that point. In other words, the velocity component normal to the moving surface at a given point determines the strength of the source at that point. If the speed of the moving surface can be represented by velocity potentials outside (Φ) and inside the body (Φ_{in}), then the strength of a source distribution can be written as

$$\sigma_m = -\left(\frac{\partial \Phi}{\partial n} - \frac{\partial \Phi_{\text{in}}}{\partial n}\right) \quad (38)$$

Substituting Eq. (38) into Eq. (35) yields

$$\sigma_m = -(\omega \times r)_p \cdot \boldsymbol{n}_p \quad (39)$$

where $\partial \Phi_{\text{in}}/\partial n = 0$ from Eq. (37) is used. In this way, the moving boundary condition can be represented by the addition of sources.

E. Combining Vortices

Two or more vortices may be amalgamated into a central vortex in numerous ways for a number of reasons,[13,14] namely, to limit the unrealistically large velocities induced in each other, to simulate more closely some merging that occurs naturally, and to reduce the computational time. Amalgamation is an approximation and there is no correct way to perform it. In addition, it is often difficult to assess the more elusive effects of merging on the numerical predictions because the problem is highly nonlinear. The consequences are intermingled with those of many other parameters and ad hoc assumptions. It has been customary to amalgamate two or more vortices into a single vortex of strength placed at the center of vorticity, given by

$$z = \sum \Gamma_j z_j \Big/ \sum \Gamma_j \quad (40)$$

In the present calculation, the total number of discrete vortices in the wake is kept at 4000. In other words, when more than 4000 vortices are present, some vortices are combined into one vortex by using Eq. (40).

F. Splitting of Vortices

In the calculation, the complete flowfield is represented only by discrete vortices. When one vortex is far away from another vortex, there is no information to represent the fluid motion between the two vortices. The method of vortex splitting is applied to gain more information about their trajectories. Mook et al.[15] suggested this method to improve the accuracy of simulating the unsteady wake behind an airfoil. The vortex splitting method used in Ref. 15 consists of splitting two vortices into three. The procedure of vortex splitting used here is illustrated in Fig. 3. Let d be the separation distance between two vortices of strengths Γ_1 and Γ_2 at time t, because d is larger than a specified critical length d_0 (here d_0 is five times the distance between the trailing edge and its nascent vortex). Before time $t + \Delta t$ is reached, two vortices of strengths Γ_1 and Γ_2 are split into five vortices of strengths equal to

$$\Gamma_{10} = \Gamma_1/3, \qquad \Gamma_{11} = \Gamma_1/3, \qquad \Gamma_{12} = (\Gamma_1 + \Gamma_2)/3$$
$$\Gamma_{21} = \Gamma_2/3, \qquad \Gamma_{20} = \Gamma_2/3 \quad (41)$$

at locations as shown in Fig. 3. This scheme is implemented in the computation.

G. Zonal Decomposition Algorithm

A disadvantage of the discrete vortex method is that its computational cost for updating the flowfield rises as the square of the number of discrete vortices. The reason is that when the time step is small

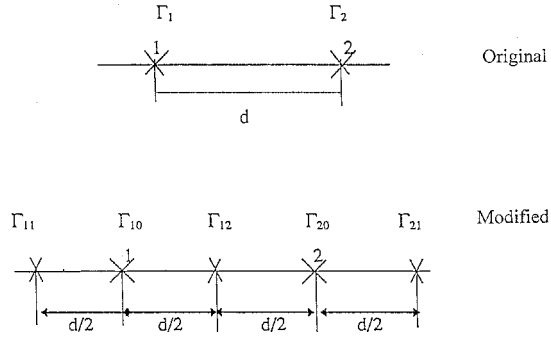

Fig. 3 Vortex splitting scheme.

and the number of vortices is too large, each vortex is influenced by the others. There are two methods for tackling this problem. One is to design a zonal decomposition algorithm[16,17] to reduce the operational cost of each time step. The other is to design a program to run on parallel-processing hardware to gain the performance benefits. In this research, the zonal algorithm was used to reduce the computational time.

Following Clarke and Tutty,[17] N_p vortices are assumed to be contained within a domain D. When sufficiently far away from D, the velocity induced by all N_p vortices may be calculated by using a Laurent series of n_t terms, where n_t depends on the accuracy required. "Sufficiently far" in this case is relative to the maximum distance from any vortex to some arbitrary point in D. This maximum distance is termed the "radius of a zone." The coefficients of the Laurent series can be calculated in advance of the summation relative to this arbitrary center point λ. Hence, beyond a certain distance from the center, the series can be used. And, if N_p is large, work is saved in comparison with direct summation over each vortex. The formulas for the coefficients, velocity, and convergence condition are

$$a_k = \sum_{j=1}^{N_p} \Gamma_j (z_j - \lambda)^{k-1} \tag{42}$$

$$u(z) - iv(z) = \frac{1}{2\pi i} \sum_{k=1}^{n_t} a_k (z - \lambda)^{-k} + \mathcal{O}(\varepsilon) \tag{43}$$

provided that

$$|z - \lambda| > h(n_t, \varepsilon) \cdot \sup(|z_j - \lambda| : j = 1, \ldots, N_p) \tag{44}$$

where a_k are the coefficients for the zone; Γ_j and z_j are, respectively, the strengths and positions of the vortices in the zone; λ is the complex center point of the zone; h is a function depending on n_t, the number of terms used in the series; and ε is the accuracy required.

H. No-Slip Condition

For simulating the flow around an airfoil with a base-vented spoiler, as shown in Fig. 4, a suitable numerical should develop, which can represent separation both upstream and downstream of the spoiler tips. Because viscosity may play an important role when the gap size is small, more careful consideration about the boundary conditions is required. Here, a method is developed to incorporate the no-slip condition on the airfoil surface.

To satisfy the no-slip condition in the calculation, an extra condition is imposed as follows:

$$\nabla\Phi \cdot \boldsymbol{\tau} = (\nabla\phi_\infty + \nabla\phi_b + \nabla\phi_w) \cdot \boldsymbol{\tau} = 0 \tag{45}$$

where $\boldsymbol{\tau}$ is a vector tangent to the airfoil and spoiler surfaces. Additional singularities represented by a vortex pair $(\Gamma'_q, -\Gamma'_q)$ have been added to both sides of each panel at a distance r_0 away from the control point C, as shown in Fig. 5. Because of the opposite sense of rotation of this vortex pair, no additional tangential velocity is introduced at the control point, but their unknown strength allows Eq. (45) to be satisfied. In addition, this vortex pair provides zero additional circulation. Note that because the velocity at the control point of each panel is zero, the surface pressure of the airfoil calculated from the unsteady Bernoulli's equation is evaluated at the point where Γ'_q is located.

By substituting all induced velocities calculated as discussed in Sec. II.A and making use of boundary conditions [Eq. (45)], two systems of linear algebraic equations for boundary vortices, shedding

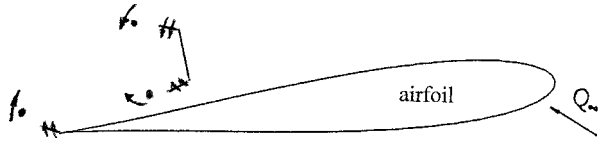

Fig. 4 Separated flow model for airfoil with base-vented spoiler.

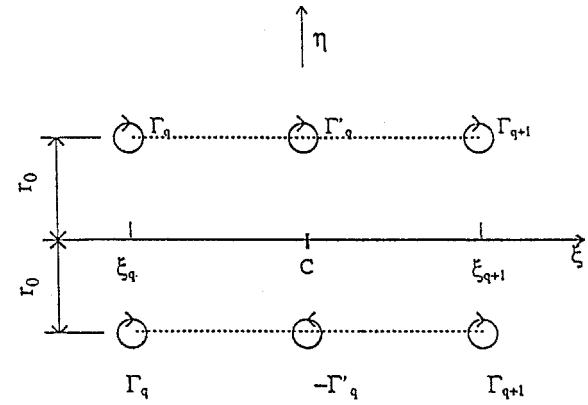

Fig. 5 Surface singularities.

vortices, and a uniformly distributed source on the airfoil surface are obtained in the following forms:

$$\sum_{q=1}^{2N+N_w} A_{pq}\Gamma_q + \sum_{q=1}^{2(N-1)} A'_{pq}\Gamma'_q + \sigma \sum_{q=1}^{N-1} B_{pq} = -[U(t) + u_w, V(t) + v_w] \cdot \boldsymbol{n}_p \tag{46}$$

$$\sum_{q=1}^{2N+N_w} C_{pq}\Gamma_q + \sum_{q=1}^{2(N-1)} C'_{pq}\Gamma'_q + \sigma \sum_{q=1}^{N-1} D_{pq} = -[U(t) + u_w, V(t) + v_w] \cdot \boldsymbol{\tau}_p \tag{47}$$

$$(u_w)_p = \sum u_{pm} = \sum \frac{\Gamma_m}{2\pi} \left[\frac{y_p - y_m}{(x_p - x_m)^2 + (y_m - y_p)^2} \right]$$
$$(v_w)_p = \sum v_{pm} = \sum \frac{-\Gamma_m}{2\pi} \left[\frac{x_p - x_m}{(x_p - x_m)^2 + (y_p - y_m)^2} \right] \tag{48}$$

where $m = 1, \ldots, N_s$, and N_s is the number of the shed vortices. $U(t)$ and $V(t)$ include the freestream velocity components and the velocity components of the moving spoiler.

I. Convection and Diffusion of Vorticity

The Navier–Stokes equations show that the velocity of a flowfield can be considered as the balance between convection and diffusion. The convection can be calculated by the influence of bound vortices, shed vortices, and sources in the flowfield. The convective components of the velocity at (x_m, y_m), due to a point vortex of unit strength at (x_n, y_n), are given by

$$U_{\Gamma mn} = -\frac{(y_m - y_n)}{2\pi\left[(x_m - x_n)^2 + (y_m - y_n)^2\right]} \tag{49}$$

$$V_{\Gamma mn} = -\frac{(x_m - x_n)}{2\pi\left[(x_m - x_n)^2 + (y_m - y_n)^2\right]} \tag{50}$$

The velocity components at (x_m, y_m) by a point source of unit strength at (x_n, y_n) are

$$U_{\sigma mn} = \frac{(x_m - x_n)}{2\pi\left[(x_m - x_n)^2 + (y_m - y_n)^2\right]} \tag{51}$$

$$V_{\sigma mn} = \frac{(y_m - y_n)}{2\pi\left[(x_m - x_n)^2 + (y_m - y_n)^2\right]} \tag{52}$$

The convection of a vortex at (x_m, y_m) may thus be calculated from all influence in the field as follows:

$$u_C = \sum_{n=1}^{2N+N_w} \Gamma_n U_{\Gamma mn} + \sum_{\substack{n=1 \\ n\neq N}}^{N_s} \Gamma_m U_{\Gamma mn} + \sum_{n=1}^{N} \sigma U_{\sigma mn} + U_\infty \quad (53)$$

$$v_C = \sum_{n=1}^{2N+N_w} \Gamma_n V_{\Gamma mn} + \sum_{\substack{n=1 \\ n\neq N}}^{N_s} \Gamma_m V_{\Gamma mn} + \sum_{n=1}^{N} \sigma V_{\sigma mn} + V_\infty \quad (54)$$

In the present calculation, the diffusive component of the velocity is also considered. Following the idea of Lewis,[18] the Navier–Stokes equations may be written as

$$\frac{\partial \omega}{\partial t} + \frac{\partial}{\partial x}\left[\left(u - \frac{\nu}{\omega}\frac{\partial \omega}{\partial x}\right)\omega\right] + \frac{\partial}{\partial y}\left[\left(v - \frac{\nu}{\omega}\frac{\partial \omega}{\partial y}\right)\omega\right] = 0 \quad (55)$$

The diffusion velocity (u_d, v_d) may be written as

$$u_d = -\frac{\nu}{\omega}\frac{\partial \omega}{\partial x} \quad (56)$$

$$v_d = -\frac{\nu}{\omega}\frac{\partial \omega}{\partial y} \quad (57)$$

where ν is the kinematic viscosity of the fluid.

The simplest viscous vortex is the Lamb vortex[14] of which the distribution of vorticity is given by

$$\omega = (\Gamma/4\pi\nu t)\exp(-r^2/4\nu t) \quad (58)$$

The tangential velocity of the vortex is maximum at $r_0 = 2.242\sqrt{(\nu t)}$, and this value is usually considered as the core of the vortex. Equation (58) is the exact solution of the Navier–Stokes equations for a single viscous vortex in an unbounded incompressible domain. The vorticity ω at (x_p, y_p), due to a system of distributed vortices of circulation Γ_m placed at (x_m, y_m), can be approximated by

$$\omega_p = \frac{1}{\pi r_0^2}\sum_m \Gamma_m \exp\left[-\frac{(x_m - x_p)^2 + (y_m - y_p)^2}{r_0^2}\right] \quad (59)$$

Therefore, (u_d, v_d) may be calculated, and the velocity of each discrete vortex is the sum of convection velocity and the diffusion velocity, i.e.,

$$u = u_C + u_d \quad (60)$$

$$v = v_C + v_d \quad (61)$$

J. Separation from Smooth Surface

The flow visualization in Ref. 7 shows that a separation bubble is located upstream of a spoiler. For the conventional spoiler, this separation only forms a recirculation region on the upper surface. This region has only a slight influence on the overall lift. Most published results indicate reasonable estimates without considering the bubble.[2,3,16] In this study, the upper surface separation is ignored in the conventional spoiler computation. In the base-vented spoiler case, however, the separation bubble will influence the flowfield behind the spoiler and its characteristics, and the overall circulation of the airfoil–spoiler configuration. Calculations show that the location of the separation point (sp) and the inclination θ_0 of the separation streamline leaving the separation point are important parameters. The location is generally a function of the Reynolds number and geometry of the airfoil–spoiler system. It may be estimated by either flow visualization or a criterion of boundary-layer separation. Although the position of separation may be influenced by the wake and becomes time-dependent, reasonable results can be obtained if it is assumed to be fixed on the airfoil surface upstream of the spoiler. In the present calculation, according to our flow visualization,[7] the location is chosen to be between $0.5c$ and $0.65c$, depending on the angle of attack and the gap size of venting. The inclination of the separation streamline leaving the separation point is chosen to be 45 deg measured with respect to the airfoil surface. If flow separates at the separation point with a local velocity v_{sp}, then a vortex sheet for shedding discrete vortices into the flowfield continuously has a strength equal to

$$\gamma_{sp} = v_{sp} \quad (62)$$

where the velocity is calculated at the point that is r_0 away from the surface. The length of the vortex sheet is equal to the length of the panel nearest the separation point.

III. Results and Discussion

The nondimensional time step $\Delta T = \Delta t\, Q_\infty/c$ of shedding vortices, which strongly influences the computational accuracy, was chosen to minimize error of the simulations. In the computations, it was selected to be between 0.005 and 0.01 for conventional spoiler cases, depending on the deployment rate of the spoiler, and to be 0.005 for all base-vented spoiler cases. The computational tests showed that any further reduction in the computational time step did not reduce the computational error.

A. Conventional Spoiler

At the first step, an 11%-thick Joukowsky airfoil fitted with an upper surface spoiler of 10% chord in length and hinged at 70% chord measured from the leading edge of the airfoil is considered. For comparing results of the present computation with the previous computations, as well as with experimental measurements, the cases of slightly raised and fully closed spoiler are assumed. Various spoiler deployment rates have been investigated in the present study. The nondimensional time between the start and finish of deployment $T_0 = t_0 Q_\infty/c$ falls in the range 0.1–5.0. These rates correspond to $\omega = 500$ deg/s of aircraft at high subsonic speeds. For testing the reliability of the present method to solve the problem with arbitrary airfoil shape, the NACA 0012 airfoil with a $10\%c$ spoiler hinged at $70\%c$ is also considered. In all studies, a constant angular velocity was assumed.

In Fig. 6, the present computed flow patterns are compared at various instants with computational results in Ref. 3 at the same tip speed

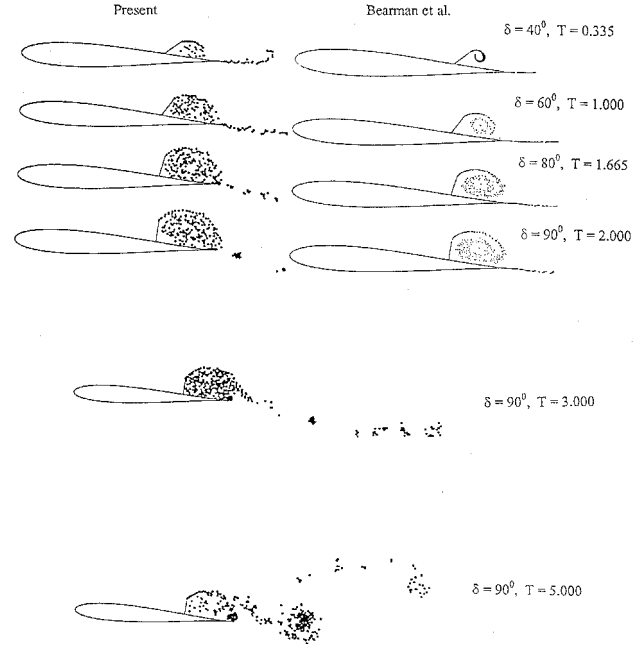

Fig. 6 Computed flow patterns at various times (δ = 30 deg → 90 deg, α = 0 deg, and u_{tip}/Q_∞ = 0.05236).

of the spoiler on the initial flow development behind the spoiler when it moves continuously from $\delta = 30$ to 90 deg at a spoiler tip velocity $u_{\text{tip}}/Q_\infty = 0.05236$ and $\alpha = 0$ deg. The computed flow patterns from present calculations are similar to the published results. Again, viscous effects and diffusion of vortices may be the causes of the difference. The computational patterns show that the shed vortices diffused more randomly than the previous computations.[3] In general, the flow patterns show that a strong vortex, which is made up of vortices shed from the spoiler tip, grows until it starts to interact with the trailing edge. The vortices from the trailing edge start to spread into the region behind the spoiler, and eventually disrupt the vortices from the spoiler tip and cause the spoiler vortices to be shed.

Figures 7 and 8 show the flow patterns at $\alpha = 0$ deg, when the spoiler angle δ changes from 10 to 30 deg at $u_{\text{tip}}/Q_\infty = 0.0174$, and when δ changes from 0 to 50 deg at $u_{\text{tip}}/Q_\infty = 0.37$. The flow development downstream of the moving spoiler is similar to that of the sudden deployment of a spoiler. The moving speed and the final inclination of the spoiler determine the strength of the gross vortex caused by spoiler deployment. The larger the spoiler angle and the faster the spoiler deployment rates, the stronger the vortex shed. Figure 9 shows a long-term-averaged pressure distribution compared with experimental mean pressure.[19] The measured and computed results are in good agreement.

Figures 10 and 11 show the transient variations of lift for the cases when δ changed from 10 to 30 deg, with $u_{\text{tip}}/Q_\infty = 0.0174$ and $\alpha = 0$ deg by the present method and Ref. 3, respectively. The general trends of the lift histories are similar to the experimental results,[20] in which lift is found to increase before decreasing to its steady-state value. Because the present method can easily reproduce the initial separated flow condition as found in the experiments, the present computational result is closer to the experimental result. The C_L reported by Bearman et al.[3] in Fig. 11 is about 0.2 higher than that from experiments. Note that the experiments[20] had a starting condition in which the spoiler was slightly raised with a preestablished separated flow before development.

Figures 12 and 13 show the transient variations of lift coefficient when the spoiler is deployed from 10 to 30 deg at $u_{\text{tip}}/Q_\infty = 0.0174$ and $\alpha = 12$ deg, and when δ is from 10 to 50 deg at $u_{\text{tip}}/Q_\infty = 0.37$ and $\alpha = 0$ deg. A short period of adverse lift is induced before the intended reduction in lift occurs. The lift history at this high rate of

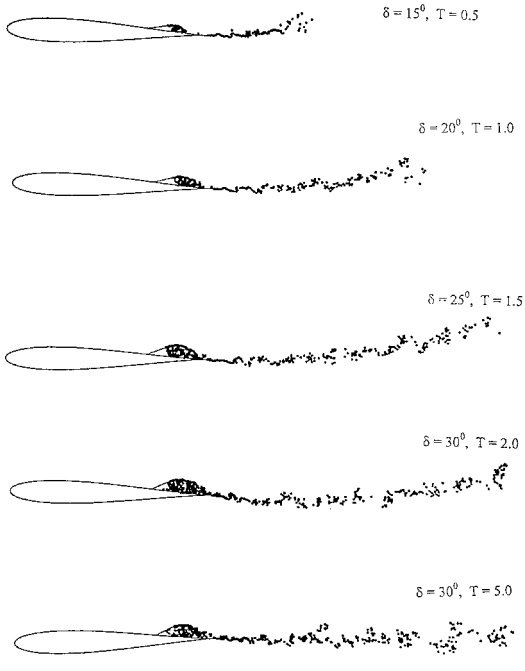

Fig. 7 Computed flow patterns at various times (δ = 10 deg → 30 deg, α = 0 deg, and u_{tip}/Q_∞ = 0.0174).

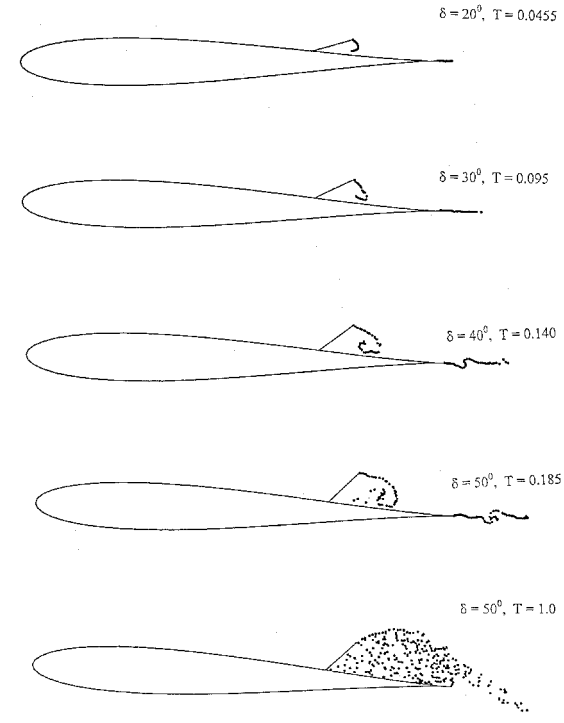

Fig. 8 Computed flow patterns at various times (δ = 10 deg → 50 deg, α = 0 deg, and u_{tip}/Q_∞ = 0.37).

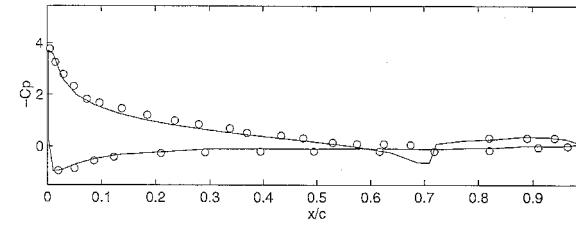

Fig. 9 Long-term pressure distributions (δ = 10 deg → 30 deg, α = 12 deg, and u_{tip}/Q_∞ = 0.0174): ——, present, and ○, experiment.[19]

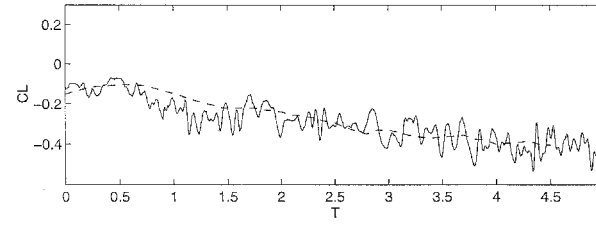

Fig. 10 Time variations of lift (δ = 10 deg → 30 deg, α = 0 deg, and u_{tip}/Q_∞ = 0.0174): ——, present, and – – –, experiment.[20]

spoiler deployment is similar to that of a suddenly deployed spoiler. Figure 14 shows the computed transient variation of the lift coefficient compared with measured results[7] for a NACA 0012 airfoil when the spoiler is rotated from 0 to 90 deg with $u_{\text{tip}}/Q_\infty = 0.25$ at $\alpha = 0$ deg. The computation agrees qualitatively with experimental measurement. Again, the phenomenon of adverse lift is predicted during the spoiler deployment.

Figure 15 shows some typical lift time histories when spoiler is opened from 10 to 50 deg at $T_0 = 0.190, 0.358$, and 4.00 at $\alpha = 0$ deg to indicate how the adverse lift and the time to reach the maximum adverse lift both depend on the spoiler deployment rate. In addition, the integration of the pressure distribution over the spoiler alone only contributes a small amount of lift ($C_L \approx -0.0023$) after the

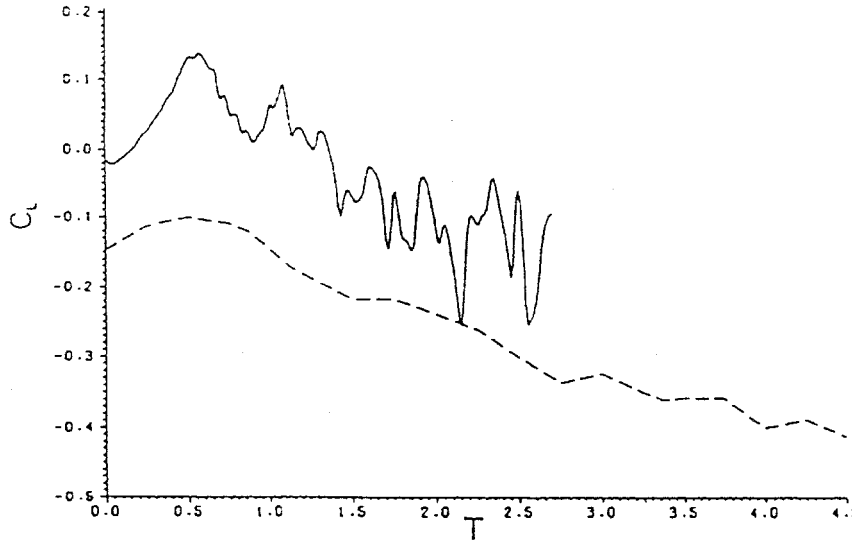

Fig. 11 Time variations of lift[3] (δ = 10 deg → 30 deg, α = 0 deg, and u_{tip}/Q_∞ = 0.0174): ——, computed,[3] and - - -, experiment.[20]

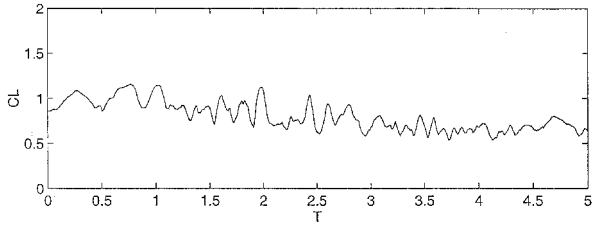

Fig. 12 Time variation of lift (δ = 10 deg → 30 deg, α = 12 deg, and u_{tip}/Q_∞ = 0.0174).

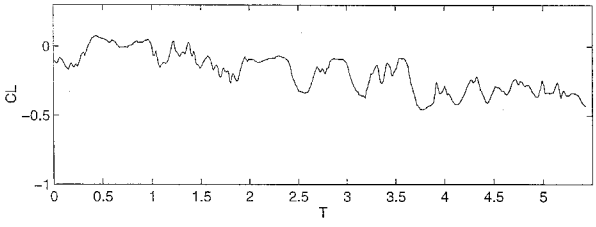

Fig. 13 Time variation of lift (δ = 10 deg → 50 deg, α = 0 deg, and u_{tip}/Q_∞ = 0.370).

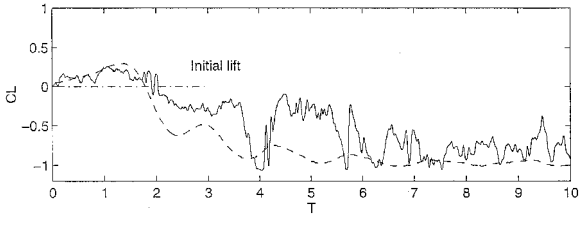

Fig. 14 Lift histories for NACA 0012 (δ = 0 deg → 90 deg, α = 0 deg, and u_{tip}/Q_∞ = 0.25): ——, present, and - - -, experiment.[3]

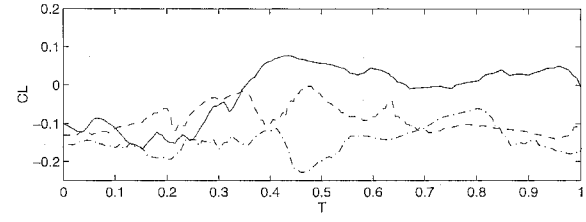

Fig. 15 Time variations of lift at different T_0 (δ = 10 deg → 50 deg, and α = 0 deg): ——, T_0 = 0.190; - - -, T_0 = 0.358; and -·-, T_0 = 4.00.

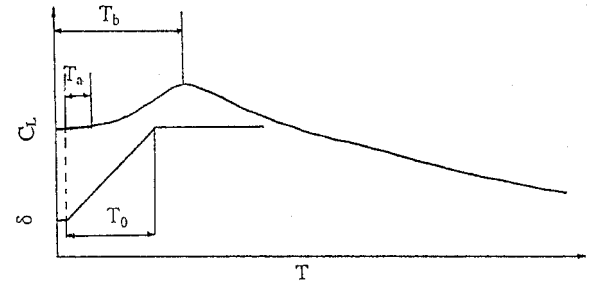

Fig. 16 Time delays in lift.

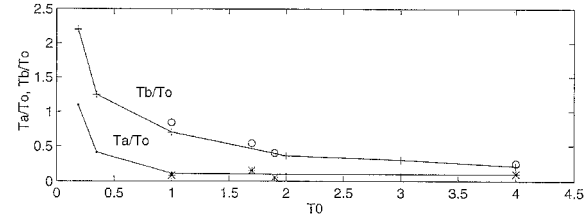

Fig. 17 Variations of time delays with spoiler deployment rate: ●, T_a/T_0 present; ∗, T_a/T_0 experiment[20]; +, T_b/T_0 present; and ○, T_b/T_0 experiment.[20]

spoiler deployment, because the suction force between the spoiler and airfoil can be counterbalanced by a similar downward force on the spoiler. The unsteady flow induced by the moving spoiler is the formation of a vortex behind the spoiler, causing a region of suction on the rear upper surface of the airfoil. The strength of this vortex depends on the spoiler deployment speed and angle. The growth of this concentrated vortex causes the lift to increase, i.e., adverse lift, until the vortex stops growing and starts to convect downstream, thus resulting in the loss of lift. The flow pattern then repeats with the development of another vortex from the spoiler, but it is less concentrated, causing another smaller rise in the lift, etc.

Calculations show that there is some delay about the change in lift when the spoiler is rapidly opened. This delay in lift can be measured with two delay times: one is time to reach the onset of lift change T_a, and the other is time to reach the maximum adverse lift T_b as shown in Fig. 16. The computed values of T_a/T_0 and T_b/T_0 are plotted against the nondimensional deployment time T_0 and compared with the experimental results[20] in Fig. 17. The trends of T_a/T_0 and T_b/T_0 are very similar, although the latter is larger in magnitude, in general. From computations, if T_0 is greater than 0.8, T_b/T_0 is usually smaller than 1. This means that the maximum adverse lift is reached before

the end of the spoiler motion. Computations show that the time to reach the maximum adverse lift depends on the velocity of the spoiler tip.

The computations show that the interaction between shedding vortices from the spoiler tip and airfoil trailing edge gives rise to a highly turbulent oscillatory wake, which may affect the performance of the airfoil. The most important effect is the adverse lift induced by the spoiler motion. One possible way to reduce the adverse lift is to introduce a gap between the spoiler and airfoil, as indicated by the flow visualization pictures in Ref. 7. Because the gap introduces another separation point near the airfoil surface, the computational model presented here requires some modifications to simulate this special kind of flow.

B. Base-Vented Spoiler

A NACA 0012 airfoil fitted with an upper surface base-vented spoiler of 10%c in length, and hinged at 70%c measured from the leading edge of the airfoil, is considered here. Because the results are compared with flow visualizations and results of force measurements,[7] the Reynolds number used in the calculation is chosen to match the experimental values, which are 1.2×10^4 and 4×10^5 in Ref. 7.

Figure 18 shows the computed flow patterns compared with visualization[7] when the spoiler is rotated from 45 to 90 deg at $u_{\text{tip}}/Q_\infty = 0.053$. The development of the flowfield around an airfoil with a moving base-vented spoiler can be described as follows. When the base-vented spoiler is opened, the shear layers from both tips of the spoiler grow asymmetrically downstream of the spoiler. The shear layer from the upper tip of the spoiler develops faster than the shear layer from the lower tip of the spoiler. The separation from the airfoil trailing edge in the case of the base-vented spoiler is similar to that of the conventional spoiler. With an asymmetric growth of the two primary shear layers behind the spoiler, two vortex patches are formed behind the base-vented spoiler and are convected downstream, leaving a steadier separated region. The numerical flow patterns obtained with the discrete vortex method are in fair agreement with the results of the flow visualization as shown in Fig. 18. The differences may be due to the fact that the spoiler rotational speed was not constant in the experiments. In addition, the finite thickness of the spoiler is not modeled in the computation.

Figure 19 shows the computed flow patterns around a base-vented spoiler with $g/c = 5\%$ at $\alpha = 0$ deg when the spoiler is rotated from 0 to 90 deg with $u_{\text{tip}}/Q_\infty = 0.37$. The calculations show that for a slowly deployed spoiler, the shed vortices from the lower tip of the spoiler may not roll up as compared with that of the fast-deployed spoiler. The separated flow from the lower tip of the spoiler through the gap is similar to the flow from a jet. This kind of flow provides fewer interactions between the shed vortices and the airfoil surface. Because the vortex roll-up is not very strong, the adverse lift is smaller than that of fast-deployed spoiler.

Figures 20 and 21 show the lift histories compared with measured results for a 10%c spoiler with $g/c = 2\%$ and $g/c = 7\%$ at $\alpha = 0$ deg, when δ is changed from 0 to 90 deg at $u_{\text{tip}}/Q_\infty = 0.30$ and $u_{\text{tip}}/Q_\infty = 0.43$. The computed and measurement lift histories show a fair agreement. The computed results show that the adverse lift decreases when the gap size is increased, confirming that the introduction of the gap reduces the adverse lift of the airfoil. Figure 22 shows the increase in C_L from the initial state to maximum adverse lift C_{La} with different gap sizes. The result shows that, when the gap size is increased, C_{La} decreases. When the gap size increases to about 5%c, which is equal to half the spoiler length, the adverse lift

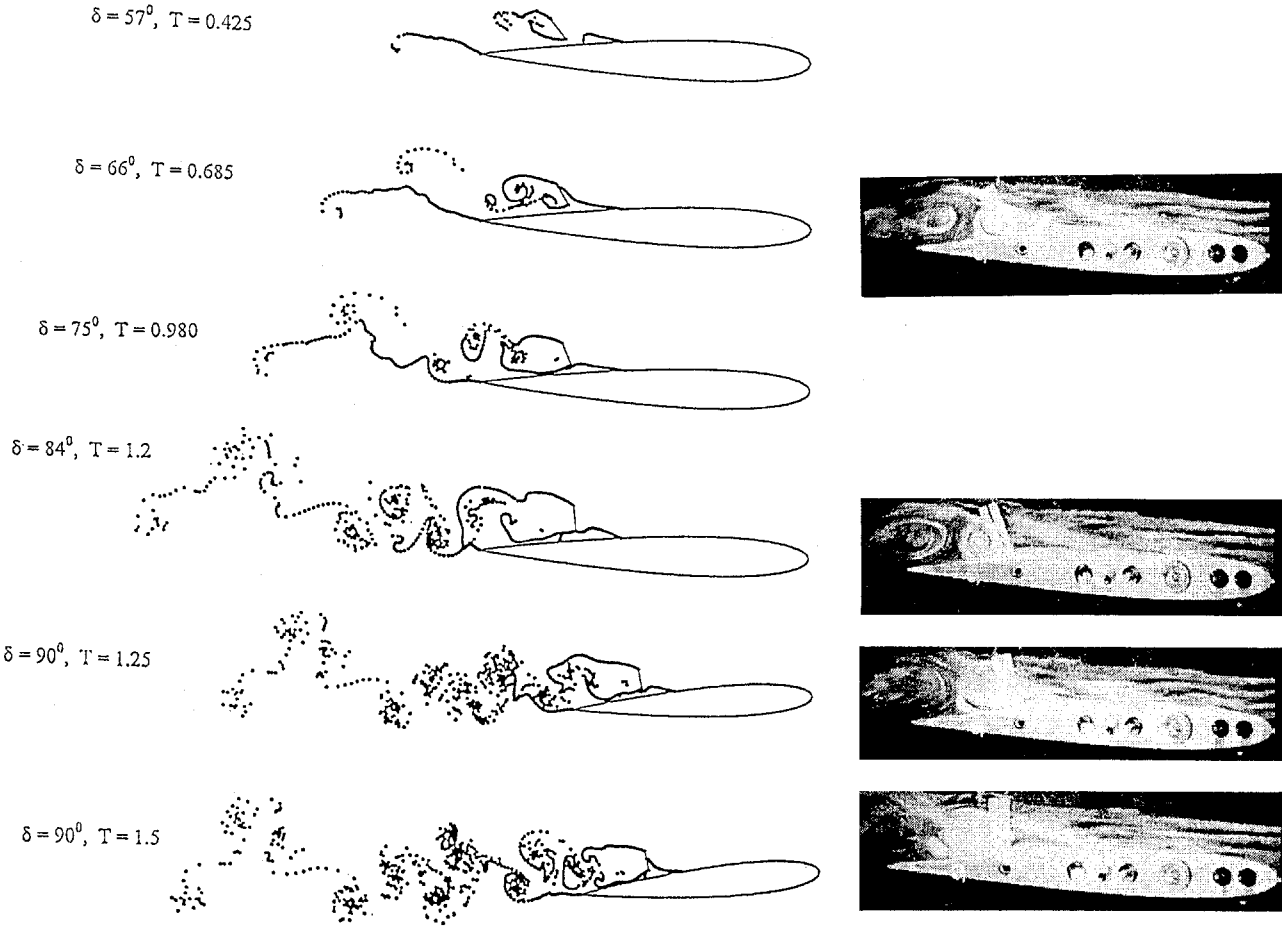

Fig. 18 Computed and flow visualization flow patterns at various times (δ = 45 deg → 90 deg, α = 0 deg, g/c = 3%, and u_{tip}/Q_∞ = 0.053).

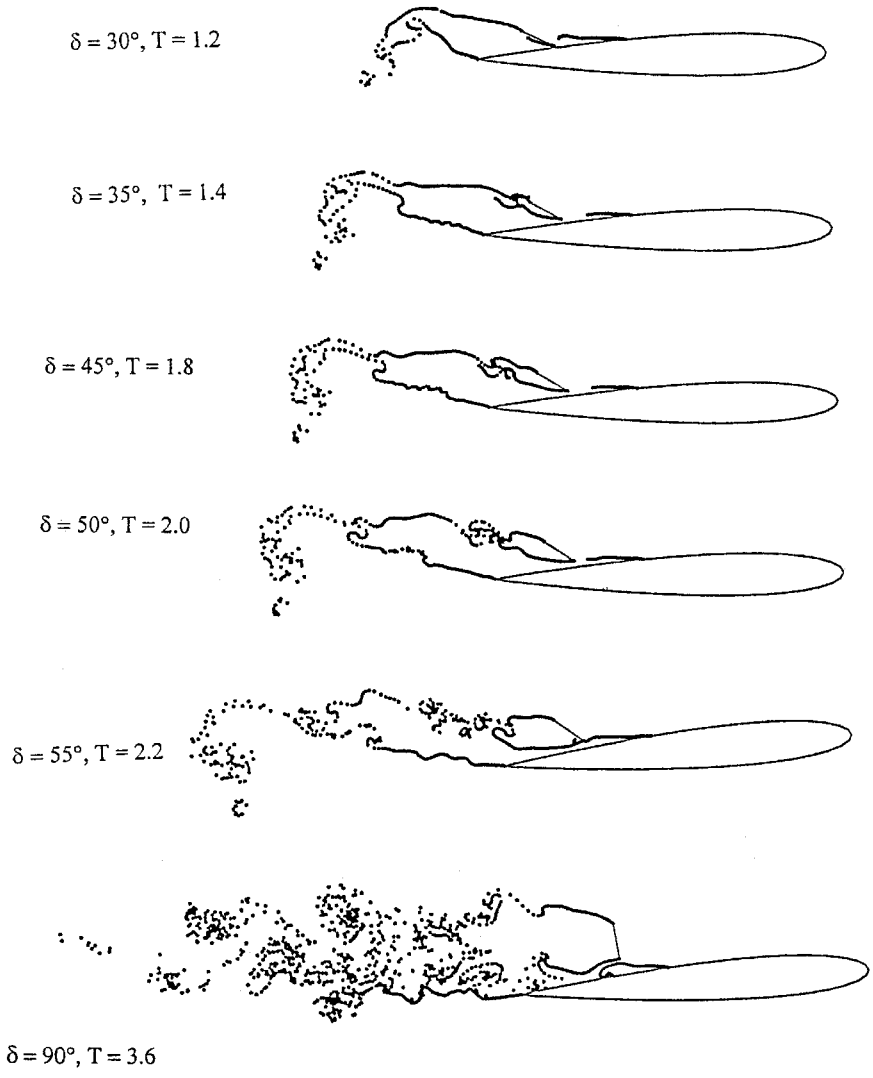

Fig. 19 Computed flow patterns at various times (δ = 0 deg → 90 deg, α = 0 deg, g/c = 5%, and u_{tip}/Q_∞ = 0.37).

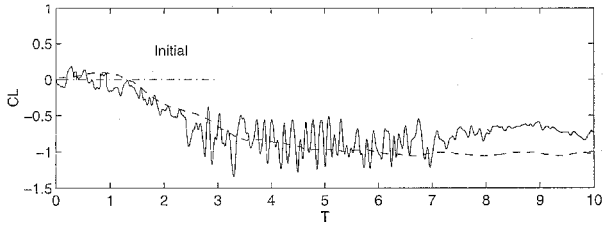

Fig. 20 Variations of C_L (δ = 0 deg → 90 deg, α = 0 deg, g/c = 2%, and u_{tip}/Q_∞ = 0.30): ——, computed, and - - -, experiment.[7]

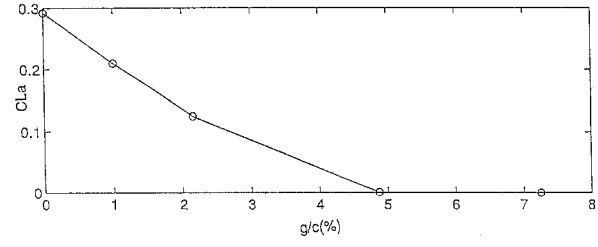

Fig. 22 Variation of maximum adverse lift with gap size at α = 0 deg, and u_{tip}/Q_∞ = 0.30.

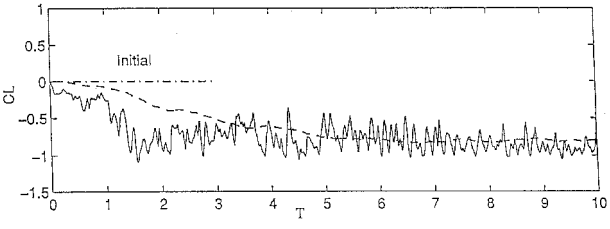

Fig. 21 Time variations of lift (δ = 0 deg → 90 deg, α = 0 deg, g/c = 7%, and u_{tip}/Q_∞ = 0.43): ——, computed, and - - -, experiment.[7]

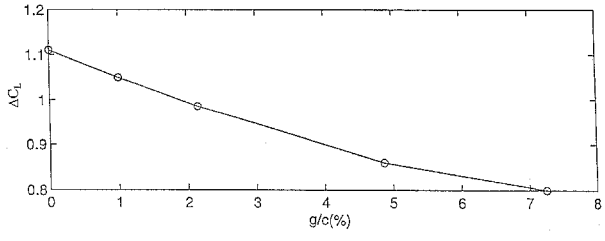

Fig. 23 Variation of adverse lift with gap size at α = 0 deg, and u_{tip}/Q_∞ = 0.30.

is negligible. This phenomenon is different from the case of sudden deployment of the base-vented spoiler, where the maximum lift does not vary much with the gap size.[7] This is most likely due to the fact that the flow at the low tip of the spoiler, does not develop fast enough in the suddenly deployed spoiler. The variations of adverse lift with the gap size are shown in Fig. 23. The variations of adverse lift, ΔC_L, i.e., $C_{L(t=0)} - C_{L(t=\infty)}$, decrease almost linearly with the increase of the gap size.

IV. Conclusions and Recommendations

A discrete vortex model has been developed to predict the unsteady separated flow behind a conventional and base-vented spoiler. The predictions in flow patterns, forces, and pressures are in reasonable agreement with experimental measurements. In the present model, the location and strength of the nascent vortices are determined separately. It clearly shows that there is an adverse lift caused by the starting vortex shed from the tip of a rapid-rotated conventional spoiler. Research in the field of viscous flow around an airfoil with a conventional spoiler is still very limited in the literature. There are two ways to simulate the viscous flow. One is to use the vortex cloud modeling, and the other is to use the computational fluid dynamics solver of the Navier–Stokes equations. Further research in these two aspects should be interesting.

The computed results of an airfoil with a base-vented spoiler show that the adverse lift is reduced when the gap size is increased, in reasonable agreement with experimental results. The flow pattern behind a base-vented spoiler is found to be quite different from that of the conventional spoiler because of the presence of the gap that allows a starting vortex to form during the rapid rotation of the spoiler. The flow through the gap acts like a jet in the long term, such that the regular vortex shedding pattern behind the conventional spoiler is disturbed. Future work should include the Navier–Stokes computations of flow patterns behind conventional and base-vented spoilers to compare with the predictions from the discrete vortex model. However, the development of efficient mesh-generation methods for moving boundaries such as the spoiler is necessary. Finally, an extension of the present two-dimensional study to the three-dimensional study will be an important contribution toward the modeling of transient aerodynamic characteristics of spoilers.

References

[1]Ghia, U., Zuo, L., and Ghia, K. N., "Analysis and Control of Unsteady Separated Flow," AIAA Paper 89-1018, Sept. 1989.

[2]Tou, H. B., and Hancock, G. J., "Part VI: The Rapid Deployment of a Spoiler on a Two-Dimensional Aerofoil," *Aeronautical Journal*, Vol. 91, No. 910, 1987, pp. 492–498.

[3]Bearman, P. W., Graham, J. M. R., and Kalkanis, P., "Numerical Simulation of Separated Flow to Spoiler Deployment," *Conference Proceedings of the Royal Aeronautical Society*, London, 1989, pp. 2.1–2.15.

[4]Abdelrahman, M. M., Ghazi, M. A., Olwi, I. A., and Al-Bahi, A. M., "Aircraft Spoiler Effects Under Wind Shear," *Journal of Aircraft*, Vol. 31, No. 1, 1994, pp. 154–160.

[5]Mabey, D. G., "A Review of Some Recent Research on Time-Dependent Aerodynamics," *Aeronautical Journal*, Vol. 98, No. 1099, 1984, pp. 23–37.

[6]Yeung, W. W. H., Xu, C., and Gu, W., "Reduction of Transient Adverse Effects of Spoilers," *Journal of Aircraft*, Vol. 34, No. 4, 1997, pp. 479–484.

[7]Xu, C., "Separated Flow Around an Airfoil with a Spoiler," Ph.D. Dissertation, Dept. of Mechanical and Production Engineering, Nanyang Technical Univ., Singapore, 1997.

[8]Clements, R. R., and Maull, D. J., "The Representation of Sheets of Vorticity by Discrete Vortices," *Progress in Aerospace Sciences*, Vol. 16, No. 3, 1975, pp. 129–146.

[9]Edwards, R. H., and Cheng, H. K., "The Separation Vortex in the Weiss-Fogh Circulation-Generation Mechanisms," *Journal of Fluid Mechanics*, Vol. 120, 1982, pp. 463–473.

[10]Hsu, A. T., and Wu, J. C., "Vortex Flow Model for the Blade-Vortex Interaction Problem," *AIAA Journal*, Vol. 26, No. 5, 1988, pp. 621–623.

[11]Lee Y. J., and Yang, J. Y., "A Panel Method for Arbitrary Moving Boundaries Problems," *AIAA Journal*, Vol. 28, No. 3, 1990, pp. 432–438.

[12]Kim, M. J., and Mook, D. T., "Application of Continuous Vorticity Panels to General Unsteady Two-Dimensional Lifting Flows," *Journal of Aircraft*, Vol. 23, No. 4, 1986, pp. 464–471.

[13]Chorin, A. J., "Numerical Study of Slightly Viscous Flow," *Journal of Fluid Mechanics*, Vol. 57, 1973, pp. 785–796.

[14]Sarpkaya, T., "Computational Method with Vortices—The 1988 Freeman Scholar Lecture," *Journal of Fluids Engineering*, Vol. 111, 1989, pp. 5–52.

[15]Mook, D. T., Roy, S., Choksi, G., and Dong, B., "Numerical Simulation of the Unsteady Wake Behind an Airfoil," *Journal of Aircraft*, Vol. 26, No. 6, 1989, pp. 1081–1089.

[16]Xu, C., and Yeung, W. W. H., "Discrete Vortex Method for Airfoil with Unsteady Separated Flow," *Journal of Aircraft*, Vol. 33, No. 6, 1996, pp. 1208–1210.

[17]Clarke, N. R., and Tutty, O. R., "Construction and Validation of a Discrete Vortex Method for the Two-Dimensional Incompressible Navier–Stokes Equations," *Computers and Fluids Journal*, Vol. 23, No. 6, 1994, pp. 751–783.

[18]Lewis R. I., *Vortex Element Method for Fluid Dynamic Analysis of Engineering Systems*, Cambridge Univ. Press, London, 1992.

[19]Parkinson, G. V., and Yeung, W., "A Wake Source Model for Airfoils with Separated Flow," *Journal of Fluid Mechanics*, Vol. 179, 1987, pp. 41–57.

[20]Kalligas, K., "A Comparative Assessment of Different Types of Rapidly Moving Spoilers at Low Airspeeds," Bristol Univ., Aeronautical Dept. Rept. on MOD Agreement, AT/2034/068, England, UK, 1986.